catalysts

MDPI

Article

Time- and Temperature-Varying Activation Energies: Isobutane Selective Oxidation to Methacrolein over Phosphomolybdic Acid and Copper(II) Phosphomolybdates

Trevor C. Brown [1,*], David J. Miron [1], Susannah L. Brown [1] and Shane M. Kendell [2]

[1] School of Science and Technology, University of New England, Armidale, NSW 2351, Australia; dmiron@une.edu.au (D.J.M.); susannah.brown3@gmail.com (S.L.B.)

[2] School of Science and Mathematics, Howard Payne University, Brownwood, TX 76801, USA; shane.kendell@gmail.com

* Correspondence: trevor.brown@une.edu.au; Tel.: +61-2-6773-2872

Academic Editors: Keith Hohn and Andreas Martin

Received: 20 June 2016; Accepted: 25 August 2016; Published: 10 September 2016

Abstract: The selective oxidation energetics of isobutane to methacrolein over phosphomolybdic acid and copper(II) phosphomolybdates have been investigated using low-pressure, pseudo-steady-state and temperature-programming techniques. Time-varying flexible least squares methods were used to determine variations in oxidation activation energies as the temperature increases at 5 °C·min^{-1}. Catalyst activity stabilizes by the fourth consecutive temperature-programmed run. Rate parameters increase linearly with temperature in two sinusoidal, oscillating wave packets. For $H_3PMo_{12}O_{40}$, three distinct reaction pathways are apparent in the fourth run with activation energies 76 ± 3, 93 ± 7 and 130 ± 3 kJ·mol^{-1}, and under these experimental conditions are observed at the optimum temperatures 704 ± 7 K, 667 ± 25 K and 745 ± 7 K, respectively. Over the copper-containing catalysts, two pathways are apparent: 76 ± 3 kJ·mol^{-1} at 665 ± 9 K and 130 ± 3 kJ·mol^{-1} at 706 ± 9 K. The three activation energies indicate either different reaction pathways leading to methacrolein or distinct active sites on the catalyst surface. The intermediate activation energy, 93 kJ·mol^{-1}, only observed over phosphomolybdic acid, may be linked to hydrogen bonding. Differences in optimum temperatures for the same activation energies for $H_3PMO_{12}O_{40}$ and for the copper catalysts indicate that compensating entropy changes are smaller over $H_3PMo_{12}O_{40}$. The inclusion of copper enhances catalyst stability and activity.

Keywords: variable activation energies; isobutane selective oxidation; methacrolein; phosphomolybdic acid; copper(II) phosphomolybdates

1. Introduction

Catalytic selective oxidation of isobutane over Keggin polyoxometalates to form methacrolein and methacrylic acid is recognized as a viable and attractive alternative to current industrial methods [1–5]. An understanding of the intrinsic physical and chemical processes of such gas–solid reactions will allow catalyst development and optimization. Solid substrates, such as phosphomolybdic acid and phosphomolybdate salts, have two roles in the catalysis, an acidic role leading to activation of C–H bonds and a selective oxidizing role to form the required products. For methacrolein formation from isobutane, four hydrogen atoms are abstracted from the isobutane, via oxidative dehydrogenation,

and one lattice oxygen is added. Three lattice oxygens [O] are used for each converted isobutane molecule:

$$(CH_3)_3\,CH + 3\,[O] \rightarrow\ CH_2\ =\ C\,(CH_3)\,CHO + 2H_2O$$

Mechanisms for methacrolein formation from isobutene over phosphomolybdate catalysts have been reviewed by Sun et al. [1]. The rate-determining step is the oxidative breaking of the C–H bond at the tertiary carbon, leading to the formation of an alkoxide group combined with a hydroxyl group. This is followed by the formation of two C–O–Mo bridges and a dioxyalkylidene intermediate. This intermediate can via C–O bond dissociation give either methacrolein or a carboxylate species when oxidized at Mo–O bonds. The carboxylate species is the precursor to methacrylic acid. Another proposed pathway includes the intermediate formation of isobutene [3]. The kinetics are not always comparable between catalytic systems, because varying activity is often observed, due to the wide range of structures, possible metals inside the phosphomolybdates, and hence wide variations in acid strength and O-atom activity. In addition, there is the likelihood of structural reorganization at different temperatures [1]. The introduction of cations can lead to multifunctionality of active sites [6] and, hence, differences in activity and selectivity. Mizuno et al. [7] have demonstrated that the substitution of Cu^{2+} into $Cs_{2.5}H_{0.5}PMo_{12}O_{40}$ gives lower yields of methacrylic acid and methacrolein from isobutane.

A low-pressure, pseudo-steady-state experimental technique has been developed to better understand the primary steps of reactions activated at the surfaces of real solid catalysts [8–10]. This technique monitors the concentrations of gas-phase reactants and products evolving from a Knudsen cell reactor via a quadrupole mass spectrometer. Molecular flow conditions are used and the temperature of the cell is raised at a linear rate and is also monitored. This increasing temperature and consequent variations in adsorption, diffusion and reaction causes perturbations to the steady-state partial pressures within the reactor. The challenge has been to determine accurate rate parameters and, in particular, the true activation energies from these data, and hence to probe the energetics of the catalytic reaction steps.

The most common method for determining rate-parameters (prefactor A and activation energy E) for gas–solid reactions is to assume an appropriate reaction model $f\,(\alpha)$, where α is reaction progress or conversion, and calculate constant rate-parameters from a fit to the experimental data [11,12]. The rate law is:

$$\frac{d\alpha}{dt} = A\exp\left(\frac{-E}{RT}\right) f\,(\alpha) \tag{1}$$

However, for gas–solid kinetics under non-isothermal, pseudo steady-state conditions, and where surface heterogeneity, activation, deactivation, simultaneous reactions, and mass transfer limitations affect apparent rate, the rate parameters are likely to vary with both time and temperature. Due to these complexities in the kinetics, temperature variations in the kinetic triplets (A_T, E_T and $f\,(\alpha_T)$) are difficult to calculate from experimental data and proposed models have been controversial [13,14]. During temperature programing, the apparent rate law at each temperature becomes:

$$\frac{d\alpha_T}{dt} = A_T\exp\left(\frac{-E_T}{RT}\right) f\,(\alpha_T) \tag{2}$$

Another consideration for activation energy variations is oscillatory behavior [15,16]. Oscillations in heterogeneous catalytic oxidation reaction rates are observed in product concentrations and may be sinusoidal, harmonic, relaxation-type or chaotic [17]. This behavior is often assigned to physical changes, such as heat and mass transport effects [15], and chemical properties, such as activation and deactivation of active sites [18].

Recently, we have used time-varying flexible least squares methods [19] to calculate variable activation energies and prefactors for isobutane cracking over zeolites [20,21] and 3-methyl-2-oxetanone

(β-lactone) desorption from phosphomolybdates [22]. Experimental data for the anaerobic selective oxidation of isobutane to methacrolein over pure phosphomolybdic acid ($H_3PMo_{12}O_{40}$), pure copper(II) phosphomolybdate ($Cu_{1.5}PMo_{12}O_{40}$) and three combined acid and copper salts: $Cu_{0.5}H_2PMo_{12}O_{40}$; $CuHPMo_{12}O_{40}$ and $Cu_{1.25}H_{0.5}PMo_{12}O_{40}$, using the low-pressure, pseudo-steady-state technique, have been previously reported [2,10]. Methacrylic acid is not observed as a product under the low-pressure conditions. The aim of this paper is to investigate the use of flexible least squares methodology to calculate variable rate parameters for methacrolein formation and thus to provide an improved understanding of the surface kinetics. Previous analyses of these data [10] have yielded single activation energies for each catalyst, as shown in Table 1. The conclusions from this earlier work are that $H_3PMo_{12}O_{40}$ is the least active catalyst at low temperatures and the most active at high temperatures, while deactivation during the 3rd and 4th runs is significant. $Cu_{1.25}H_{0.5}PMo_{12}O_{40}$ is the most selective for methacrolein formation at low temperatures.

Table 1. Apparent activation energies calculated for the selective oxidation of isobutane to methacrolein over phosphomolybdic acid and copper(II) phosphomolybdates, reproduced with permission from [10]. Copyright Elsevier, 2008.

Catalyst	Temperature (°C)	E_{app} (kJ·mol^{-1})
$H_3PMo_{12}O_{40}$	246–451	99.3 ± 1.1
$Cu_{0.5}H_2PMo_{12}O_{40}$	353–502	61.3 ± 1.8
$CuHPMo_{12}O_{40}$	325–501	58.4 ± 0.9
$Cu_{1.25}H_{0.5}PMo_{12}O_{40}$	329–501	52 ± 4
$Cu_{1.5}PMo_{12}O_{40}$	342–500	75.4 ± 1.2

2. Results

2.1. Temperature-Programmed, Low-Pressure, Pseudo Steady-State Methacrolein Formation

Kendell et al. [2,10] have previously reported experimental data obtained for anaerobic isobutane reactions over phosphomolybdic acid and copper(II) phosphomolybdates. Mass spectral abundances for β-lactone, acetic acid, carbon dioxide and water, produced during oxidation over all catalysts, were also monitored and recorded over the measured temperature range. For each catalyst, four consecutive and equivalent temperature-programmed runs were undertaken on each sample. Resultant mass-spectral profiles for the first two to three runs were inconsistent, due to adsorbed water and other calcination effects leading to significant variations in the rates [10]. As a consequence, the 4th temperature programmed runs are the focus of these analyses, although the 3rd runs have been included. This instability is not apparent in the early runs for zeolite catalysis [22] under these low-pressure conditions. Hence, the rate of reduction or phosphomolybdate active sites to 4th run stable structures is slow.

Typical profiles for isobutane and methacrolein mass spectral abundances during temperature programming are shown in Figure 1. These data are from the 3rd temperature-programmed run of isobutane over $H_3PMo_{12}O_{40}$. The raw data are denoised using wavelet methods [23] (red lines in Figure 1). For this purpose, R programming language [24] is used with the package "WaveThresh" [25]. Discrete wavelet transforms are applied to mass spectral abundances using the Daubechies Least Asymmetric wavelet family, with a range of vanishing moments. Weighted averages of the wavelet denoised values are used in all analyses.

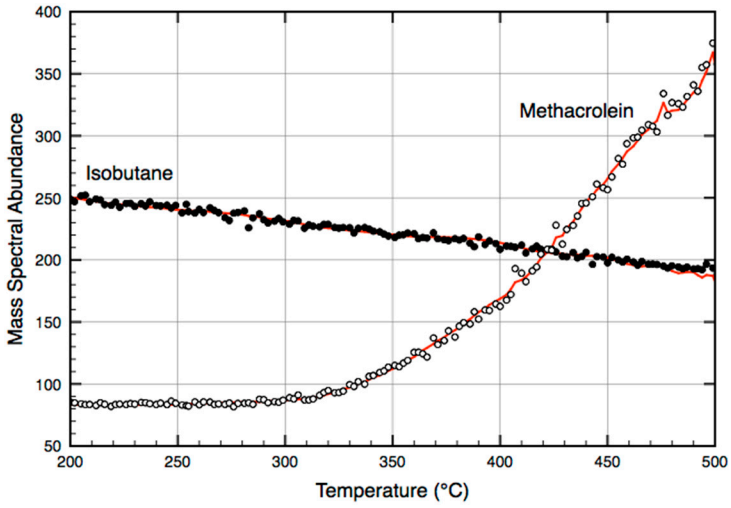

Figure 1. Isobutane mass spectral abundance (filled circles) and methacrolein abundance (open circles) as a function of temperature, both with weight average wavelet denoised lines (red lines) during temperature-programmed oxidation of isobutane over phosphomolybdic acid (3rd run).

2.2. Rate Parameters from Temperature-Programmed, Low-Pressure Experiments

For these temperature-programmed, low-pressure, pseudo steady-state experiments, the rate law (Equation (2)) may be written:

$$\frac{\mathrm{d}\,[\mathrm{Ma}]}{\mathrm{d}t} = A_T \exp\left(\frac{-E_T}{RT}\right) f\left([\mathrm{Ia}]\right) \tag{3}$$

Here, [Ma] and [Ia] are the concentrations of methacrolein and isobutane within the Knudsen cell. The reaction model, $f\left([\mathrm{Ia}]\right)$, is the surface coverage of isobutane at each temperature. At low pressures, coverage is often assumed to be proportional to reactant pressures. However, isobutane concentrations at active sites are not likely to be uniformly distributed across the surface or within the catalyst bulk and may not be directly proportional to the concentrations within the Knudsen cell. As a consequence, the reaction order, n_T, is included in the rate law and adjusted to account for the variations in surface coverage.

$$\frac{\mathrm{d}\,[\mathrm{Ma}]}{\mathrm{d}t} = A_T \exp\left(\frac{-E_T}{RT}\right) [\mathrm{Ia}]^{n_T} \tag{4}$$

Methacrolein mass spectral abundances at m/e = 70, I_{70} are proportional to the mass spectral sensitivity factor α_{70}, escape rate constants from the Knudsen cell, $k_{\mathrm{esc,\,Ma}}$ and methacrolein concentration within the cell. Abundance is also proportional to the rate of evolution of methacrolein:

$$I_{70} = \alpha_{70}\, k_{\mathrm{esc,Ma}}\, [\mathrm{Ma}] = \alpha_{70} \frac{\mathrm{d}\,[\mathrm{Ma}]}{\mathrm{d}t} \tag{5}$$

The analogous equation can be written for the measured isobutane abundances with concentration [Ia] at m/e = 58, I_{58}:

$$I_{58} = \alpha_{58}\, k_{\mathrm{esc,Ia}}\, [\mathrm{Ia}] \tag{6}$$

Isobutane escape rate constants are a function of temperature, Knudsen cell dimensions and molecular flow constants $(A_{\mathrm{esc,\,Ia}})$ [26]:

$$k_{\mathrm{esc,Ia}} = A_{\mathrm{esc,Ia}} T^{1/2} \tag{7}$$

Combining Equations (4)–(7), and taking the natural log, gives the following linear equations with three parameters at each temperature, A_T, E_T and n_T:

$$\ln I_{70} = \ln A_T - \frac{E_T}{RT} + n_T \ln\left(\frac{I_{58}}{\alpha_{58} A_{\mathrm{esc,Ia}} T^{1/2}}\right) + \ln\alpha_{70} \quad (8)$$

Apparent activation energies, E_T are combinations of the energetics of adsorption, diffusion, reaction and desorption elementary steps. Apparent prefactors, A'_T with unit s^{-1}, are also combinations of these steps, as well as the coverage terms and constants in Equation (8) and are:

$$\ln A'_T = \ln A_T + n_T ln\left(\frac{I_{58}}{\alpha_{58} A_{\mathrm{esc,Ia}} T^{1/2}}\right) + \ln\alpha_{70} \quad (9)$$

2.3. Calculating Time- and Temperature-Varying Activation Energies

Time-varying flexible least squares (TVFLS) is used to determine the three rate parameters, E_T, prefactors, ln A_T and exponent, n_T by fitting Equation (8) to the temperature-programmed data [22]. This methodology is a generalization of ordinary linear regression with the inclusion of time-variant regression parameters. TVFLS code has been provided by Kalaba and Tesfatsion [19] and adapted for the statistical computing language R [25]. TVFLS exactly simulates a data set (ln I_{70}, $1/RT$ and ln $\left(I_{58}/T^{1/2}\right)$) by varying the three rate parameters at each temperature. Windows of 20 data points (ca. 33 °C) across the full range of temperatures were TVFLS simulated, with the the midpoint within each window used in the fitting. Final fitted parameters are unique and have been shown to exhibit negligible cost functions [24]. An example of fitted parameters are plotted against temperature in Figure 2 for methacrolein evolution over phosphomolybdic acid during the 3rd temperature-programmed run.

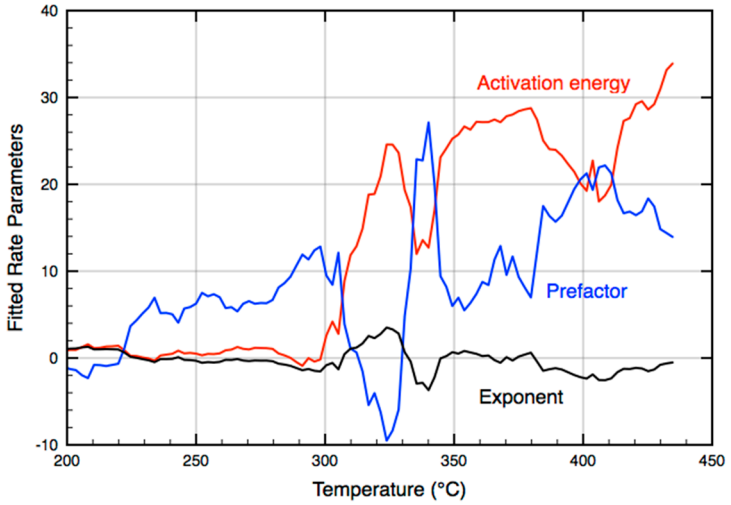

Figure 2. Apparent activation energies, E_T (red line), prefactors, ln A_T (blue line) and exponent, n_T (black line) as a function of temperature for the evolution of methacrolein during temperature-programmed oxidation of isobutane over phosphomolybdic acid (3rd run).

The baselines for isobutane and methacrolein mass spectral abundances, used in these calculations are non-zero. As a consequence, the small or zero activation energies at temperatures less than 300 °C in Figure 2 reflect experimental variations at baselines, rather than a consequence of surface reactions. The apparent activation energies and prefactors are adjusted for this baseline by subtracting the apparent prefactor, ln A'_{T_0} (Equation (9)), when the fitted activation energy is zero from the apparent rate coefficient:

$$\ln k'_{T,\text{true}} = \ln\left(A'_T - A'_{T_0} - \frac{E_T}{RT}\right) = \ln A'_{T,\text{true}} - \frac{E_{T,\text{true}}}{RT} \quad (10)$$

Arrhenius plots of $\ln k'_{T,\text{true}}$ against $1/T$ then allows for the calculation of true, apparent activation energies, $E_{T,\text{true}}$ and prefactors, $\log_{10} A'_{T,\text{true}}$, as demonstrated in Figure 3. As is clear from this figure, a plot of the apparent $\log_{10} A'_{T,\text{true}}$ against $E_{T,\text{true}}$ would yield an approximately straight line. The method of Invariant Kinetic Parameters [27] relates heating rate-dependent activation energies with prefactors for non-isothermal data. The resultant linear relationship between the two rate parameters gives an equation with compensation parameters m and c:

$$\log_{10} A'_{T,\text{true}} = mE_{T,\text{true}} + c \quad (11)$$

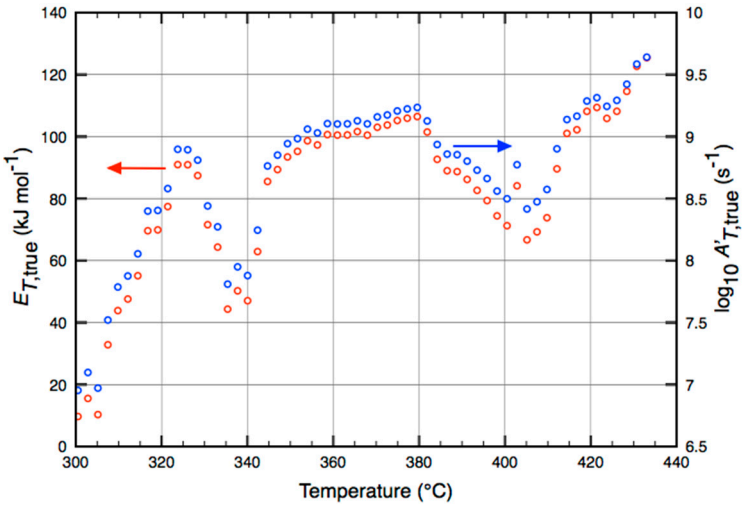

Figure 3. Apparent activation energies, $E_{T,\text{true}}$ (red circles) and prefactors, $\log_{10} A'_{T,\text{true}}$ (blue circles) plotted against temperature for the evolution of methacrolein during temperature-programmed oxidation of isobutane over phosphomolybdic acid (3$^{\text{rd}}$ run).

This compensation effect highlights the challenge in determining the true activation energies and prefactors. Rate coefficients for selective oxidation can be simplified to Equation (12) where the rate coefficient ratio of activated complex to surface diffusion away from active sites control the temperature-dependence [21].

$$k'_{T,\text{true}} = \frac{k_{T,\text{oxidation}}}{k_{T,\text{diffusion}}} \quad (12)$$

Assuming no other activated steps at these high temperatures, the likely selective oxidation activation energies are $E_{T,\text{true}} = E_{T,\text{oxidation}} - E_{T,\text{diffusion}}$.

3. Discussion

3.1. High-Temperature, Average Rate-Parameters for Methacrolein Formation

Three temperature regions, low, medium, and high, with different apparent activity for methacrolein formation are apparent during temperature-programmed oxidation [2,10,28]. The low-temperature region is assigned to methacrolein desorption. Here, methacrolein precursors have been trapped or adsorbed on or within the catalyst. The medium-temperature region is where activation energies are negative. This corresponds to declining methacrolein pressures within the Knudsen cell as temperature increases. Negative activation energies may indicate competing reactions (e.g., formation of β-lactone [29]), secondary methacrolein reactions on the catalyst surface

(e.g., dimerization), or the formation of metastable states. Activation energy distributions in the high-temperature region, for all catalysts are investigated in this paper, and have been the focus of previous analyses [2,10]. Here, the mass-spectral signal is large and sensitive to variations in activity. The kinetics of this region is associated with the reaction dynamics of selective and partial oxidation of isobutane to methacrolein.

Table 2 lists minimum and maximum activation energies for each run calculated using TVFLS across the high-temperature region for each of the phosphomolybdic acid, copper(II) phosphomolybdate and mixed copper/Brønsted acid catalysts. As Figures 4–7 also show, parameters fluctuate over the high-temperature range and in most cases there is an overall increase with increasing temperature. Activation energies cover very broad ranges for each catalyst with standard deviations varying from 27 to 35 kJ·mol^{-1} and, thus, average values have limited significance.

Table 2. Range of and average activation energies and prefactors for the selective oxidation of isobutane to methacrolein over phosphomolybdic acid, copper(II) phosphomolybdates and mixed copper/Brønsted acid catalysts in the high-temperature region.

Catalyst	Temperature (°C)	$\log_{10} A'_{T,\text{true}}$ (s^{-1})	$E_{T,\text{true}}$ (kJ·mol^{-1})	
			Min–Max	Average
3rd Run				
$H_3PMo_{12}O_{40}$	300–433	8.7 ± 0.6	10–125	82 ± 27
$CuHPMo_{12}O_{40}$	310–435	8.3 ± 0.6	21–139	82 ± 31
$Cu_{1.25}H_{0.5}PMo_{12}O_{40}$	307–435	8.4 ± 0.6	24–128	83 ± 30
$Cu_{1.5}PMo_{12}O_{40}$	311–438	7.8 ± 1.0	23–120	63 ± 30
4th Run				
$H_3PMo_{12}O_{40}$	359–479	8.9 ± 0.8	15–153	91 ± 35
$Cu_{0.5}H_2PMo_{12}O_{40}$	320–435	8.1 ± 0.7	20–134	72 ± 33
$Cu_{1.25}H_{0.5}PMo_{12}O_{40}$	308–433	8.3 ± 0.5	22–134	78 ± 32
$Cu_{1.5}PMo_{12}O_{40}$	316–436	8.8 ± 1.4	22–139	76 ± 35

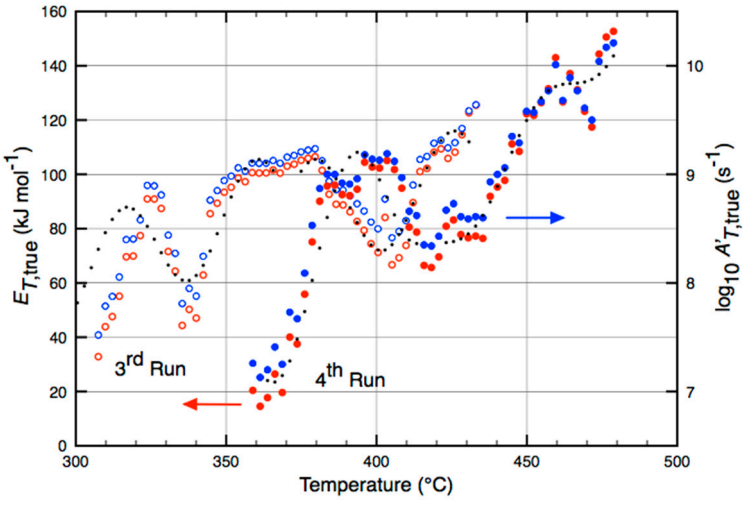

Figure 4. Apparent activation energies, $E_{T,\text{true}}$ (red circles) and prefactors, $\log_{10} A'_{T,\text{true}}$ (blue circles) plotted against temperature for the evolution of methacrolein during temperature-programmed oxidation of isobutane over phosphomolybdic acid for the 3$^{\text{rd}}$ (unfilled circles) and 4$^{\text{th}}$ runs (filled circles). Black dots are simulated activation energy oscillations.

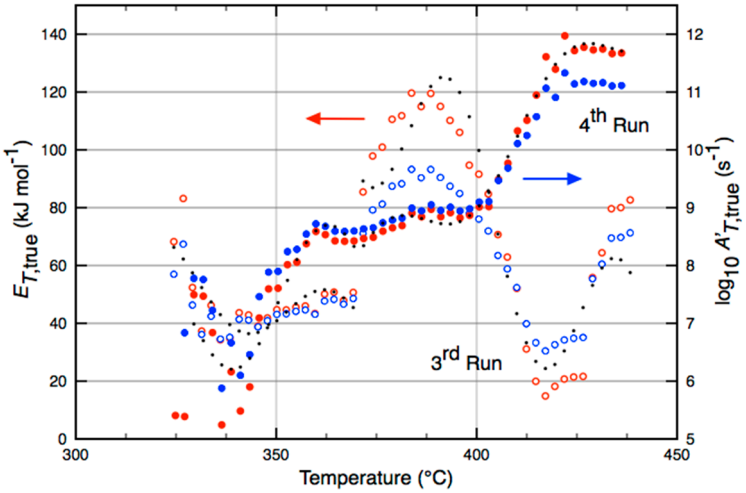

Figure 5. Apparent activation energies, $E_{T,\text{true}}$ (red circles) and prefactors, $\log_{10} A'_{T,\text{true}}$ (blue circles) plotted against temperature for the evolution of methacrolein during temperature-programmed oxidation of isobutane over copper(II) phosphomolybdate ($Cu_{1.5}PMo_{12}O_{40}$) for the 3rd (unfilled circles) and 4th runs (filled circles). Black dots are simulated activation energy oscillations.

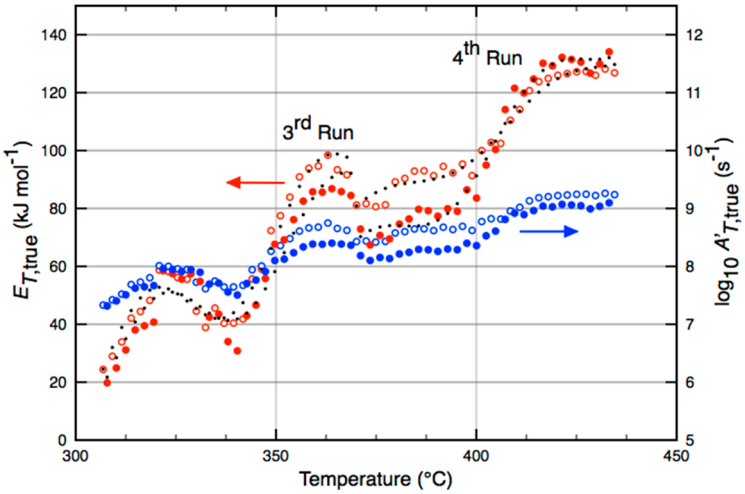

Figure 6. Apparent activation energies, $E_{T,\text{true}}$ (red circles) and prefactors, $\log_{10} A'_{T,\text{true}}$ (blue circles) plotted against temperature for the evolution of methacrolein during temperature-programmed oxidation of isobutane over $Cu_{1.25}H_{0.5}PMo_{12}O_{40}$ for the 3rd (unfilled circles) and 4th runs (filled circles). Black dots are simulated activation energy oscillations.

Temperature ranges listed in Table 2 are similar for all runs except the 4th run over $H_3PMo_{12}O_{40}$, where activity is apparent from 359 to 479 °C. For the 3rd run, activation energies and prefactors are negligible up to ca. 307 °C, and only very small amounts of methacrolein evolve. As a consequence, the heating ramp was continued for an additional 46 °C and 4th run average rate parameters are larger than calculated for all the other runs. This surface is, energetically, the least active.

The 3rd run for $Cu_{1.5}PMo_{12}O_{40}$ has smaller average rate parameters and suggests that this surface is the most active. To confirm this, much higher abundances are observed for methacrolein formation over $Cu_{1.5}PMo_{12}O_{40}$ than over all other catalysts. That is, the high pressures of methacrolein form across the full temperature range. Differences in average parameters for consecutive runs for both $H_3PMo_{12}O_{40}$ and $Cu_{1.5}PMo_{12}O_{40}$ demonstrate poor catalyst stability. For all other runs, catalyst temperature ranges and average rate parameters are similar, although the 3rd run optimum activation energies are typically 5 to 10 kJ·mol^{-1} higher than for the 4th runs, suggesting increased activity. Mixed

copper/Brønsted acid catalysts are most stable, showing similar activity for both the 3rd and 4th runs. Activation energies reported by Kendell et al. [10], and listed in Table 1, lead to similar conclusions for the activity of $H_3PMo_{12}O_{40}$ and $Cu_{1.5}PMo_{12}O_{40}$. Reported average activation energies for the mixed catalysts, however, are much lower than the optimum magnitudes shown in Table 2.

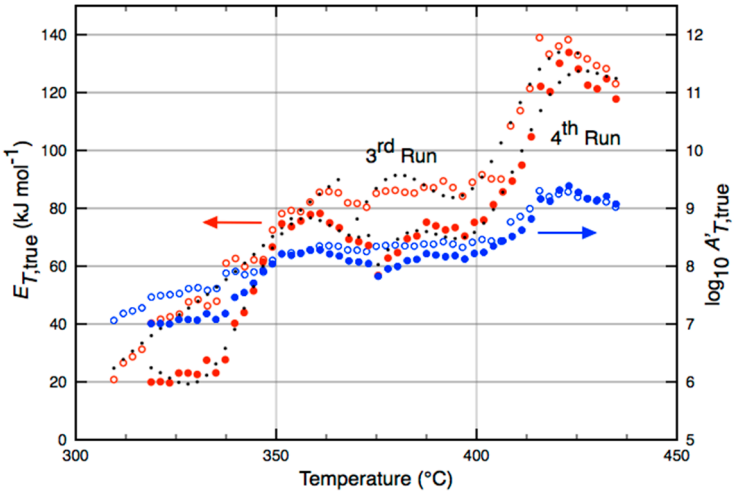

Figure 7. Apparent activation energies, $E_{T,true}$ (red circles) and prefactors, $\log_{10} A'_{T,true}$ (blue circles) plotted against temperature for the evolution of methacrolein during temperature-programmed oxidation of isobutane over $CuHPMo_{12}O_{40}$ for the 3rd run (unfilled circles) and over $Cu_{0.5}H_2PMo_{12}O_{40}$ for the 4th run (filled circles). Black dots are simulated activation energy oscillations.

3.2. Detailed Rate-Parameter Distributions for Methacrolein Formation

More information can be obtained from a detailed investigation of the rate parameter peaks and troughs, calculated using TVFLS and plotted in Figures 4–7. Red circles in all these figures are true apparent activation energies, $E_{T,true}$, blue circles are compensating true apparent prefactors, $\log_{10} A'_{T,true}$ and black dots are simulated sinusoidal waves that are discussed in Section 3.3.

Figure 4 is a plot of rate parameters against furnace temperature for methacrolein formation over $H_3PMo_{12}O_{40}$ for the 3rd and 4th temperature-programmed runs. Activity commences at different temperatures for the two runs. After an initial spike in rate parameters during the 3rd run (Figure 4) they stabilize from 347 °C and then drift higher, before a steep decline at 403 °C, and then another rise from 414 °C. Average activation energies and prefactors for these maxima and minima are listed in Table 3. Similar variations are observed for the 4th run, with the top and bottom of steps reached at higher temperatures than for the 3rd run: 381, 413 and 450 °C.

Rate parameter profiles for methacrolein formation over copper(II) phosphomolybdate are shown in Figure 5. High-temperature activation commences at around 325 °C for both runs. The 3rd run profile and both phosphomolybdic acid (Figure 4) profiles differ from other profiles. Each has temperature ranges where parameters decrease, stabilize, and then increase again. During the 3rd run over $Cu_{1.5}PMo_{12}O_{40}$ there are two distinct troughs, commencing at 331 °C and at 414 °C. Corresponding average rate parameters are listed in Table 3. Each minimum is followed by rate parameter peaks at around 386 °C and 434 °C and are also listed in Table 3. During the 4th run, two upward steps are apparent. The first step reaches a maximum from 357 °C and drifts up until 403 °C, while the second maximum is from 417 °C. Significant variations in the profiles between the 3rd and 4th runs for $H_3PMo_{12}O_{40}$ and $Cu_{1.5}PMo_{12}O_{40}$ demonstrate that the catalysts deactivate during proceeding temperature-programmed runs; due, either to restructuring caused by elevated temperatures, or the reduction of accessible oxygen active sites.

Table 3. Average apparent activation energies and prefactors for distinct maxima and minima during the selective oxidation of isobutane to methacrolein over phosphomolybdic acid and copper(II) phosphomolybdates. Reaction *Types I* to *V* are regions with similar average activation energy magnitudes.

Catalyst	Temperature (°C)	$\log_{10} A'_{T,\text{true}}$ (s^{-1})	$E_{T,\text{true}}$ (kJ·mol^{-1})	Reaction *Type*
		3rd Run		
$H_3PMo_{12}O_{40}$	345–384	$10^{9.1 \pm 0.1}$	99 ± 9	*III*
	387–412	$10^{8.7 \pm 0.2}$	80 ± 8	*II*
	414–433	$10^{9.3 \pm 0.2}$	111 ± 9	*IV*
$CuHPMo_{12}O_{40}$	351–406	$10^{8.34 \pm 0.07}$	85 ± 4	*III*
	413–435	$10^{9.04 \pm 0.04}$	131 ± 6	*I*
$Cu_{1.25}H_{0.5}PMo_{12}O_{40}$	353–399	$10^{8.6 \pm 0.1}$	90 ± 5	*III*
	413–435	$10^{9.2 \pm 0.03}$	126 ± 2	*I*
$Cu_{1.5}PMo_{12}O_{40}$	331–369	$10^{7.1 \pm 0.2}$	44 ± 5	*V*
	379–393	$10^{9.5 \pm 0.1}$	115 ± 4	*IV*
	414–427	$10^{6.7 \pm 0.1}$	19 ± 3	*V*
	429–438	$10^{8.3 \pm 0.3}$	73 ± 12	*II*
		4th Run		
$H_3PMo_{12}O_{40}$	381–408	$10^{9.0 \pm 0.1}$	98 ± 5	*III*
	413–435	$10^{8.6 \pm 0.1}$	76 ± 6	*II*
	450–479	$10^{9.8 \pm 0.2}$	131 ± 10	*I*
$Cu_{0.5}H_2PMo_{12}O_{40}$	351–402	$10^{8.1 \pm 0.1}$	72 ± 5	*II*
	416–435	$10^{9.2 \pm 0.1}$	125 ± 5	*I*
$Cu_{1.25}H_{0.5}PMo_{12}O_{40}$	352–400	$10^{8.3 \pm 0.1}$	79 ± 6	*II*
	414–433	$10^{9.04 \pm 0.04}$	130 ± 3	*I*
$Cu_{1.5}PMo_{12}O_{40}$	357–403	$10^{8.8 \pm 0.2}$	74 ± 4	*II*
	417–436	$10^{11.1 \pm 0.1}$	134 ± 3	*I*

Average rate parameters for the three mixed copper/Brønsted acid catalysts have been analysed for methacrolein production: $Cu_{0.5}H_2PMo_{12}O_{40}$, $CuHPMo_{12}O_{40}$ and $Cu_{1.25}H_{0.5}PMo_{12}O_{40}$ are shown in Figures 6 and 7. Activation energies and prefactors again fluctuate and rise with increasing temperature. For all runs, activity commences from around 307 °C. Rate parameters show two clear top steps and commence at similar temperatures for all runs. This structure is also seen for the 4th run over $Cu_{1.5}PMo_{12}O_{40}$ (Figure 5). Average maxima are listed in Table 3. Activation energies and prefactors are generally higher for the 3rd runs when compared with the 4th runs, as previously noted for the average parameters, listed in Table 2. Overall increasing activation energies during each run indicate structural reorganization [1] with sites becoming less active with increasing temperature. While decreasing activation energies from the 3rd to the 4th run indicate that sites are activated or become accessible. No clear minima are apparent, however, there are dips in rate parameters that maybe better deconvoluted if different heating rates are employed.

A closer look at the rate parameter magnitudes for the peaks and troughs listed in Table 3 indicates that there are five reaction *Types*. Two of these *Types* are in six of the eight temperature-programmed runs, one in four of the runs, and another two in one or two of the runs. The two most reproducible reaction *Types* are observed in all the stabilized 4th runs.

Type I is in six runs (all except for the 3rd runs over $H_3PMo_{12}O_{40}$ and $Cu_{1.5}PMo_{12}O_{40}$) and average rate coefficients are:

$$\log_{10} k'_{T,\text{true}} = \log_{10} 9.6 \pm 0.8\ \text{s}^{-1} - \frac{130 \pm 3\ \text{kJ·mol}^{-1}}{RT} \quad (13)$$

These activation energies are therefore characteristic of methacrolein formation over stabilized copper and acidic phosphomolybdates and represent selective oxidation (minus diffusion) at accessible active sites. They are significantly higher than the previously reported magnitudes [2,10] that are averaged over the full high-temperature range and listed in Table 1. Of particular note is the large prefactor ($10^{11.1-0.1}$ s^{-1}) for the 4th run over pure $Cu_{1.5}PMo_{12}O_{40}$. This suggests enhanced accessibility and hence coverage of the active sites in the absence of Brønsted acidity.

Type II is in six runs (all the 4th runs and for the 3rd runs over $H_3PMo_{12}O_{40}$ and $Cu_{1.5}PMo_{12}O_{40}$) and measured at lower temperatures than for *Type I*:

$$\log_{10} k'_{T,\text{true}} = \log_{10} 8.5 \pm 0.3\ s^{-1} - \frac{76 \pm 3\ \text{kJ·mol}^{-1}}{RT} \quad (14)$$

These energy barriers are also therefore characteristic of methacrolein formation over stabilized phophomolybdate catalysts and more closely match the average values listed in Tables 1 and 2.

Types I and *II* rate parameters are indicative of two distinct pathways or one pathway at two different O-atom sites on stabilized phosphomolybdate catalysts [1].

Type III is in four runs (all the 3rd runs, except for $Cu_{1.5}PMo_{12}O_{40}$ and for the 4th run over $H_3PMo_{12}O_{40}$):

$$\log_{10} k'_{T,\text{true}} = \log_{10} 8.8 \pm 0.3\ s^{-1} - \frac{93 \pm 7\ \text{kJ·mol}^{-1}}{RT} \quad (15)$$

Type III rate coefficients during the 3rd runs are over similar temperatures ranges to the *Type II* 4th runs and the magnitudes are higher by ca. 17 kJ·mol^{-1}. As these equivalent parameters are observed over catalysts with significant Brønsted acidity, this pathway may include adsorption of the reactive species via hydrogen bonding [30].

Reaction *Types IV* and *V* are calculated parameters within the 3rd temperature-programed runs over $H_3PMo_{12}O_{40}$ and $Cu_{1.5}PMo_{12}O_{40}$. These are catalyst surfaces that have not been stabilized and are reaction pathways are more difficult to assign. *Type IV* are ca. 20 kJ·mol^{-1} larger than the *Type III* and so may follow a similar mechanism at weaker oxide sites. The *Type V* low activation energies may be physically adsorbed or trapped products or particularly active sites that are present in the absence of Brønsted acidity. Neither *Type* is observed during the 4th run.

Type IV is in two runs (3rd runs over $H_3PMo_{12}O_{40}$ and $Cu_{1.5}PMo_{12}O_{40}$):

$$\log_{10} k'_{T,\text{true}} = \log_{10} 9.4 \pm 0.1\ s^{-1} - \frac{113 \pm 3\ \text{kJ·mol}^{-1}}{RT} \quad (16)$$

Type V is the average of two minima in the 3rd run over $Cu_{1.5}PMo_{12}O_{40}$:

$$\log_{10} k'_{T,\text{true}} = \log_{10} 6.9 \pm 0.3\ s^{-1} - \frac{32 \pm 18\ \text{kJ·mol}^{-1}}{RT} \quad (17)$$

3.3. Oscillations in High-Temperature Activation Energies

The plots in Figures 4–7 show some oscillatory behavior [15,16], as sometimes observed in heterogeneous catalytic oxidation product reactions [17]. This is likely to be a consequence of heat and mass transport effects [15], as well as activation and deactivation of active sites [18]. Fluctuations in activation energy within the high-temperature regions, plotted in Figures 4–7 can be effectively simulated with sinusoidal wave packets (amplitude A_{osc} and reduced wavelength B_{osc}), combined with linear functions (slope C_{osc} and intercept D_{osc}) to account for the increasing energies:

$$E_{T,\text{osc}} = A_{\text{osc}} \sin\left(\frac{2\pi T}{B_{\text{osc}}}\right) + C_{\text{osc}} T + D_{\text{osc}} \quad (18)$$

Generalized reduced gradient methods [31] are used to optimize the four parameters in the nonlinear Equation (18) for each catalyst and temperature programmed run. Optimized values are listed in Table 4.

Table 4. Oscillation parameters from Equation (18) fitted to flexible least square activation energies for the selective oxidation of isobutane to methacrolein over the $[PMo_{12}O_{40}]^{3-}$ catalysts.

Catalyst	Temperature (°C)	A_{osc} (kJ·mol^{-1})	B_{osc} (K)	C_{osc} (kJ·mol^{-1}·K^{-1})	D_{osc} (kJ·mol^{-1})
3rd Run					
$H_3PMo_{12}O_{40}$	307–368	18	44	0.40	−58
	370–435	19	46	0.23	0.074
$CuHPMo_{12}O_{40}$	310–366	1.2	44	1.2	−334
	368–425	13	43	1.1	−320
$Cu_{1.25}H_{0.5}PMo_{12}O_{40}$	307–368	15	44	1.1	−298
	370–435	5.0	45	0.88	−249
$Cu_{1.5}PMo_{12}O_{40}$	313–369	12	44	−0.45	202
	372–438	33	43	−1.5	669
4th Run					
$H_3PMo_{12}O_{40}$	359–421	28	47	1.1	−340
	423–479	9.0	44	1.3	−484
$Cu_{0.5}H_2PMo_{12}O_{40}$	319–373	14	43	1.2	−358
	375–435	12	41	1.3	−454
$Cu_{1.25}H_{0.5}PMo_{12}O_{40}$	308–371	14	44	0.93	−263
	374–433	9.6	45	1.3	−415
$Cu_{1.5}PMo_{12}O_{40}$	316–369	20	44	0.40	−93
	372–436	13	46	1.3	−430

Two consecutive single wavelength sinusoidal waves are required to fit each high-temperature region data set, because in the middle of each temperature programmed run there is a discontinuous wave function (extended plateau or jump in activation energies). Equation (18) wave simulations are plotted with TVFLS data in Figures 4–7 for $H_3PMo_{12}O_{40}$, $Cu_{1.5}PMo_{12}O_{40}$, $Cu_{1.25}H_{0.5}PMo_{12}O_{40}$ and combined $Cu_{0.5}H_2PMo_{12}O_{40}$/$CuHPMo_{12}O_{40}$, respectively. Of the 16 data sets (i.e., two waves for each of the eight runs), only the first sinusoidal wave for the 3rd runs over both $H_3PMo_{12}O_{40}$ (Figure 4) and $Cu_{1.5}PMo_{12}O_{40}$ (Figure 5) does not closely match TVFLS activation energies.

All fitted sinusoidal reduced wavelengths (B_{osc}) are similar with mean 44.2 ± 1.5 °C. This similarity is likely to be a direct consequence of the experimental pseudo steady-state, low-pressure conditions, because heating and flow rates are equivalent for all runs and each wave is fitted to a similar temperature range (60 ± 4 K). The other three parameters, amplitude A_{osc}, slope C_{osc} and intercept D_{osc} are related to the catalyst and the associated reaction energetics. These parameters, listed in Table 4 show consistent magnitudes for a large majority of the runs.

Amplitudes, A_{osc} provide information on the range of reaction pathways and active sites available for selective oxidation to methacrolein. Observed maxima, minima and sinusoidal transitions correspond to the sequential sampling of reaction pathways and sites during temperature programming. Generally lowest activation energy formation occurs first, followed by higher energy formations until maximum activation energy is reached. As temperature increases, higher energy sites become available and reactant molecules adsorb at the active sites and thus the sinusoidal cycle starts again. Large amplitudes, A_{osc} typically greater that 15 kJ·mol^{-1} correspond to sampling of broad distributions of active sites with variable activity and a broad range of chemical and physical competing processes, including highly active oxidation sites, as temperature increases. Largest amplitudes are

calculated for the 3rd and 4th runs over $Cu_{1.5}PMo_{12}O_{40}$ (33 and 20 kJ·mol^{-1}) and the 4th runs over $H_3PMo_{12}O_{40}$ (28 kJ·mol^{-1}). The smallest amplitude is for the 3rd run over $CuHPMo_{12}O_{40}$.

Slope, C_{osc} is greater than zero for all catalysts except for the 3rd run over $Cu_{1.5}PMo_{12}O_{40}$ (-0.45 and -1.5 kJ·mol^{-1}·K^{-1}). Positive C_{osc} indicates that the most active sites react first, followed by higher activation energy sites or reaction *Types* with increasing temperature. For negative C_{osc} oxidation to methacrolein more active sites are exposed or form as temperature increases. Mean activation energies at each temperature and for each wave packet are calculated when $A_{osc} = 0$:

$$(E_{T,osc})_{mean} = C_{osc}T_{mean} + D_{osc} \quad (19)$$

The range of energy barriers at each temperature is $\pm A_{osc}$ (i.e., when $\sin(2\pi T/B_{osc}) = \pm 1$). The 4th temperature-programmed runs give the most reproducible results across all the catalysts, suggesting that the activity has stabilized. *Type I* and *II* regions are within the second wave packets for each of the 4th runs and *Type III* within the first wave packet for $H_3PMo_{12}O_{40}$ only. Listed in Table 5 are the averaged values of C_{osc} and D_{osc} from Table 4, activation energies from Equations (13)–(15) and the optimum temperature, T_{mean} for each *Type*. Optimum temperature highlights the activity differences between $H_3PMo_{12}O_{40}$ and the copper-containing catalysts. While *Types I* and *II* have similar activation energies, the associated methacrolein formation is apparent at higher temperatures over $H_3PMo_{12}O_{40}$. That is, reaction steps or active sites are equivalent, while the copper-containing catalysts are more active. Additionally, optimum temperatures for *Types II* and *III* over $H_3PMo_{12}O_{40}$ matches *Types I* and *II* over the copper-containing catalysts. This maybe coincidental, although demonstrates that the compensating entropy change to the activated complex is smaller over $H_3PMo_{12}O_{40}$ for equivalent reaction pathways.

Table 5. Characteristic temperatures, T_{mean} for *Types I*, *II* and *III* calculated from Equation (19) using parameters from the 4th temperature-programmed runs for the selective oxidation of isobutane to methacrolein over the $[PMo_{12}O_{40}]^{3-}$ catalysts.

Catalyst	Reaction	C_{osc}	D_{osc}	$(E_{T,osc})_{mean}$	T_{mean}
		(kJ·mol^{-1}·K^{-1})	(kJ·mol^{-1})	(kJ·mol^{-1})	(K)
$H_3PMo_{12}O_{40}$	*Type I*	1.3	−484	130 ± 3	745 ± 7
	Type II	1.3	−484	76 ± 3	704 ± 7
	Type III	1.1	−340	93 ± 7	667 ± 25
$Cu_{0.5}H_2PMo_{12}O_{40}$ $Cu_{1.25}H_{0.5}PMo_{12}O_{40}$ $Cu_{1.5}PMo_{12}O_{40}$	*Type I*	1.3	−433	130 ± 3	706 ± 9
	Type II	1.3	−433	76 ± 3	665 ± 9

4. Materials and Methods

The apparatus and experimental techniques of temperature-programmed, low-pressure, pseudo steady-state gas/solid reactions have previously been described [9,10]. In summary, a molecular flow of isobutane collides, adsorbs on and reacts with the surface of ca. 0.3 g of the catalyst located in a Knudsen cell reactor. Steady-state is initially achieved by allowing the isobutane to flow for typically 2 h at 100 °C, before initiating a linear heating-rate of 5 °C·min^{-1} to 500 °C. Isobutane and product molecules eventually escape from the Knudsen cell via an exit aperture, and are detected by a Hewlett-Packard 5995 quadrupole mass spectrometer. Isobutane is monitored by the parent peak (m/e = 58), while products are detected using characteristic peaks: m/e = 70 for methacrolein. For all catalysts, the apparent gas-phase products are methacrolein, carbon dioxide, water, acetic acid and a β-lactone. Propene, isobutene, 2-methyl-1-propanol and methacrylic acid are not detected by the mass spectrometer. The absence of these expected products is likely to be a consequence of the low isobutane conversion under the low-pressure anaerobic conditions.

Kendell et al. [2,10] have previously provided details of the reaction materials used in the experiments and the following is a summary. Instrument grade isobutane and possible gas-phase products were from Brin's Oxygen Company (BOC Gases, Australia) and are used without further purification. Flow rates and mass-spectral sensitivities of products were measured using the vapor of liquid samples from Sigma–Aldrich Pty. Ltd. (Sydney, Australia). Hydrated phosphomolybdic acid ($H_3[PMo_{12}O_{40}]\cdot 28H_2O$) and all other reagents used in the preparation of the copper salts were from Sigma–Aldrich. The copper(II) salts were prepared by dissolving 12.747 g of $H_3[PMo_{12}O_{40}]\cdot 28H_2O$ in 20.0 mL of water and adding either 0.684, 1.368, 1.707 or 2.052 g of $CuSO_4\cdot 5H_2O$. Equal molar quantities of dried $BaCO_3$ were then added to the dissolved solution to precipitate the sulfate. The resultant slurry was stirred at 55 °C for 2 h and, upon cooling, the $BaSO_4$ was removed by filtration. Four copper-containing catalysts were the obtained by evaporating the water at 55 °C to yield green solids—$Cu_{0.5}H_2PMo_{12}O_{40}$, $CuHPMo_{12}O_{40}$, $Cu_{1.25}H_{0.5}PMo_{12}O_{40}$, and $Cu_{1.5}PMo_{12}O_{40}$. The low-symmetry crystalline structures and compositions of these salts were confirmed by X-ray diffraction and fluorescence.

5. Conclusions

TVFLS has been used to calculate variable rate parameters for methacrolein formation over phosphomolybdic acid ($H_3PMo_{12}O_{40}$), copper(II) phosphomolybdate ($Cu_{1.5}PMo_{12}O_{40}$) and three combined acid and copper catalysts: $Cu_{0.5}H_2PMo_{12}O_{40}$; $CuHPMo_{12}O_{40}$; $Cu_{1.25}H_{0.5}PMo_{12}O_{40}$. The experimental data and alternate analyses have been previously reported [2,10]. Data include reactant (isobutane) and product (methacrolein) pressures, evolving from the solid catalysts contained in a Knudsen cell reactor, and monitored by a quadrupole mass spectrometer as a function of rising temperature. Data from the 3rd and 4th temperature-programmed runs are investigated and final conclusions are taken from the 4th run activation energies. This is because initial runs do not give reproducible rate parameter distributions due to impurities and the need for active site reduction and restructuring under the low-pressure conditions. Repeated dehydration and reduction of the surfaces stabilizes the catalysts.

Activation energies increase linearly in sinusoidal, oscillating wave packages as the temperature increases and have been fitted with Equation (18) for each stabilized catalyst and temperature-programmed run. Increasing energies demonstrate the broad range of catalytic active sites and environments, as well as surface restructuring and deactivation with increasing temperature. Peaks and troughs in the 4th temperature-programmed runs are assigned to two reaction *Types*. *Type I*, with activation energy 130 ± 3 kJ·mol^{-1} and *Type II*, 76 ± 3 kJ·mol^{-1} are observed for all catalysts. Under low-pressure conditions, for $H_3PMo_{12}O_{40}$ both these steps are apparent at higher optimum temperatures (745 ± 7 K and 704 ± 7 K) than for the mean of the copper-containing catalysts (706 ± 9 K and 665 ± 9 K). Given the equivalent activation energies for all catalysts, the entropy changes to activated complexes must be greater for the copper-containing catalysts. *Type III* reactions (93 ± 7 kJ·mol^{-1} and 667 ± 9 K) are only observed over $H_3PMo_{12}O_{40}$ (4th run) and are likely to be linked to the Brønsted acidity of this catalyst.

The reproducibility of mixed copper/Brønsted acid catalyst activity from the 3rd to the 4th runs (magnitudes and oscillations) demonstrate that stability is reached after only two runs, and so are considered more stable than the pure $H_3PMo_{12}O_{40}$ and $Cu_{1.5}PMo_{12}O_{40}$. Additionally, characteristic temperature ranges for the same reaction pathways over pure $H_3PMo_{12}O_{40}$ indicate lower selective-oxidation, catalytic activity than for all the copper-containing catalysts.

Acknowledgments: The authors acknowledge funding from the UNE received to support this research project and SLB thanks the School of Science and Technology for funding over summer to undertake the calculations and analysis.

Author Contributions: T.C.B. and S.M.K. conceived and designed the experimental technique and with S.M.K. performed the experiments; D.J.M. proposed and developed the code for wavelet deshrinking and time-varying flexible least-squares methods; T.C.B. and S.L.B. undertook the calculations and analyses; T.C.B. wrote the paper.

Conflicts of Interest: The authors declare no conflict of interest.

References

1. Sun, M.; Zhang, J.; Putaj, P.; Caps, V.; Lefebvre, F.; Pelletier, J.; Basset, J.-M. Catalytic Oxidation of Light Alkanes (C_1–C_4) by Heteropoly Compounds. *Chem. Rev.* **2014**, *114*, 981–1019. [CrossRef] [PubMed]
2. Kendell, S.M.; Nguyen, N.H.; Brown, T.C. Electronic Activity Relationship for Methacrolein Formation Over 4th Period Transition Metal Phosphomolybdates. *Catal. Lett.* **2013**, *143*, 61–70. [CrossRef]
3. Huynh, Q.; Shuurman, Y.; Delichere, P.; Loridant, S.; Millet, J.M.M. Study of Te and V as counter-cations in Keggin type phosphomolybdic polyoxometalate catalysts for isobutane oxidation. *J. Catal.* **2009**, *261*, 166–176. [CrossRef]
4. Jing, F.; Katryniok, B.; Dumeignil, F.; Bordes-Richard, E.; Paul, S. Catalytic selective oxidation of isobutane to methacrylic acid on supported $(NH_4)_3HPMo_{11}VO_{40}$ catalysts. *J. Catal.* **2014**, *309*, 121–135. [CrossRef]
5. Jing, F.; Katryniok, B.; Dumeignil, F.; Bordes-Richard, E.; Paul, S. Catalytic selective oxidation of isobutane over $Cs_x(NH_4)_{3-x}HPMo_{11}VO_{40}$ mixed salts. *Cat. Sci. Technol.* **2014**, *4*, 2938–2945. [CrossRef]
6. Grasselli, R.K. Fundamental principles of selective heterogeneous catalysis. *Top. Catal.* **2002**, *21*, 79–88. [CrossRef]
7. Mizuno, N.; Tateishi, M.; Iwamoto, M. Direct oxidation of isobutane into methacrylic acid and methacrolein over $Cs_{2.5}Ni_{0.08}$-substituted $H_3PMo_{12}O_{40}$. *J. Chem. Soc. Chem. Commun.* **1994**, 1411–1412. [CrossRef]
8. Sun, Y.; Brown, T.C. Catalytic cracking, dehydrogenation, and aromatization of isobutane over Ga/HZSM-5 and Zn/HZSM-5 at low pressures. *Int. J. Chem. Kinet.* **2002**, *87*, 467–480. [CrossRef]
9. Le Minh, C.; Brown, T.C. Rate parameters from low-pressure steady-state protolytic cracking and dehydrogenation of isobutane over zeolite catalysts. *Appl. Catal.* **2006**, *310*, 145–154. [CrossRef]
10. Kendell, S.M.; Brown, T.C.; Burns, R.C. Accurate low-pressure kinetics for isobutane oxidation over phosphomolybdic acid and copper(II) phosphomolybdates. *Catal. Today* **2008**, *131*, 526–532. [CrossRef]
11. Khawam, A.; Flanagan, D.R. Solid-State Kinetic Models: Basics and Mathematical Fundamentals. *J. Phys. Chem. B* **2006**, *110*, 17315–17328. [CrossRef] [PubMed]
12. Tan, G.; Wang, Q.; Zheng, H.; Zhao, W.; Zhang, S.; Liu, Z. Concept of Variable Activation Energy and Its Validity in Nonisothermal Kinetics. *J. Phys. Chem. A* **2011**, *115*, 5517–5524. [CrossRef] [PubMed]
13. Khawam, A.; Flanagan, D.R. Basics and applications of solid-state kinetics: A pharmaceutical perspective. *J. Pharm. Sci.* **2006**, *95*, 472–498. [CrossRef] [PubMed]
14. Arshad, M.A.; Maaroufi, A-K. An innovative reaction model determination methodology in solid state kinetics based on variable activation energy. *Thermochim. Acta* **2014**, *360*, 25–35. [CrossRef]
15. Imbihil, R.; Ertl, G. Oscillatory Kinetics in Heterogeneous Catalysis. *Chem. Rev.* **1995**, *95*, 697–733. [CrossRef]
16. Rosenthal, D. Functional surfaces in heterogeneous catalysis: A short review. *Phys. Status Solidi* **2011**, *208*, 1217–1222. [CrossRef]
17. Kaichev, V.V.; Gladjy, A.Y.; Prosvirin, I.P.; Saraev, A.A.; Hävecker, M.; Knop-Gericke, A.; Schlögl, R.; Bukhtiyarov, V.I. In situ XPS study of self-sustained oscillations in catalytic oxidation of propane over nickel. *Surf. Sci.* **2013**, *609*, 113–118. [CrossRef]
18. Kokkofitis, C.; Stoukides, M. Rate and oxygen activity oscillations during propane oxidation on Pt/YSZ. *J. Catal.* **2006**, *243*, 428–437. [CrossRef]
19. Kalaba, R.; Tesfatsion, L.C. Time-varying linear regression via flexible least squares. *Comput. Math. Appl.* **1989**, *17*, 1215–1245. [CrossRef]
20. Le Minh, C.; Alanazi, A.K.; Miron, D.J.; Brown, T.C. Carbon–Carbon Bond Cleavage and Dehydrogenation of Isobutane Over HZSM-5 at Low Pressures and Temperatures. *Catal. Lett.* **2012**, *142*, 1470–1473. [CrossRef]
21. Brown, T.C.; Miron, D.J.; Alanazi, A.K.; Le Minh, C. Rate Parameter Distributions for Isobutane Dehydrogenation and Isobutene Dimerization and Desorption over HZSM-5. *Catalysts* **2013**, *3*, 922–941. [CrossRef]
22. Miron, D.J.; Kendell, S.M.; Munshi, A.M.; Alanazi, A.K.; Brown, T.C. Time-Varying Flexible Least Squares for Thermal Desorption of Gases. *Int. J. Chem. Kinet.* **2013**, *45*, 374–386. [CrossRef]
23. Percival, D.B.; Walden, A.T. *Wavelet Methods for Time Series Analysis*; Cambridge University Press: New York, NY, USA, 2006.

24. R Core Team. *R: A Language and Environment for Statistical Computing*; R Foundation for Statistical Computing: Vienna, Austria, 2012.
25. Nason, G. Wavethresh: Wavelet Statistics and Transforms, version 4.6.2. Available online: http://cran.rproject.org/web/packages/wavethersh/index.html (accessed on 2 April 2013).
26. Golden, D.M.; Spokes, G.N.; Benson, S.W. Very low-pressure pyrolysis (VLPP). A versatile kinetic tool. *Angew. Chem. Int. Ed.* **1973**, *12*, 534–546. [CrossRef]
27. Budrugeac, P. Some methodological problems concerning nonisothermal kinetic analysis of heterogeneous solid-gas reactions. *J. Therm. Anal. Calorim.* **2007**, *89*, 143–151. [CrossRef]
28. Kendell, S.M.; Brown, T.C. Comprehensive Study of Isobutane Selective Oxidation Over Group I and II Phosphomolybdates: Structural and Kinetic Factors. *Catal. Lett.* **2011**, *141*, 1767–1785. [CrossRef]
29. Nguyen, N.H.; Kendell, S.M.; Le Minh, C.; Brown, T.C. Mechanistic Investigation into the Rearrangement of Lactone into Methacrylic Acid over Phosphomolybdic Acid Catalyst. *Catal. Lett.* **2010**, *136*, 28–34. [CrossRef]
30. Deshlahra, P.; Iglesia, E. Methanol Oxidative Dehydrogenation on Oxide Catalysts: Molecular and Dissociative Routes and Hydrogen Addition Energies as Descriptors of Reactivity. *J. Phys. Chem. C* **2014**, *118*, 26115–26129. [CrossRef]
31. Kemmer, G.; Keller, S. Nonlinear least-squares data fitting in Excel spreadsheets. *Nat. Protoc.* **2010**, *5*, 267–281. [CrossRef] [PubMed]